

Hypocenter location using hodogram analysis of noisy 3C microseismograms

Lejia Han, Joe Wong, and John C. Bancroft

ABSTRACT

Hodogram analysis and back-azimuth projection is one method used for mapping microseismic hypocenter locations in a homogeneous isotropic velocity field. The method works well when the input microseismograms have high signal-to noise ratios. However, when there are high levels of random noise on the raw seismograms, the mapping accuracy decreases significantly. To suppress noise and increase signal-to-noise ratios (SNRs) before hodogram/back-azimuth analysis, we applied frequency domain filtering, time domain windowing, trace averaging, and signal-noise separation (NSS). After noise suppression, the back-azimuth method coupled with statistical averaging of raypath intersections produces reasonably accurate hypocenter locations.

INTRODUCTION

Microseismic monitoring is being used increasingly to study processes in which high pressure-fluids are pumped into deep underground reservoirs. In reservoir stimulation, hydraulic fracturing is used to crack oil- and gas-bearing formations and thus increase permeability and the flow of oil and gas to flow into the producing well. Microseismic monitoring helps reservoir engineers evaluate the effectiveness of reservoir stimulation by hydraulic fracturing (Maxwell and Urbancic, 2001).

In CO₂ sequestration, carbon dioxide is forced into porous formations under high pressure. It is important to have a method for tracking the movement of CO₂ into the formation. As the gas is forced into the rock, it produces microseisms that can be detected by arrays of 3C geophones. Monitoring the microseisms and locating the hypocenters of these microseisms is equivalent to mapping the movement of the gas.

Microseismic monitoring and mapping have applications in various other fields as well. To meet regulatory requirements in oil-sands development, it is used to detect and locate events such as well-casing failure, cement cracking, and fluid release. In development of a hot-dry-rock geothermal reservoir, tracking the progress of hydraulic fracturing can be done by microseismic hypocenter mapping (Block et al., 1994). Applications of microseismic monitoring includes detection of man-made fault activation caused by deep injection of waste fluids, tracking of steam injection thermal fronts, monitoring excavation stability in nuclear waste repositories, and detection of rock burst activity in the mining industry (Oye and Roth, 2003). In fact, any process that causes sharp stress release and cracking in rock formations can be detected with microseismic monitoring and located with hodogram/back-azimuth analysis.

For monitoring a hydraulic fracturing treatment in a production well, an array of 3C seismic sensors is usually deployed in the observation well for a specific period, i.e., for several hours before treatment begins, during the treatment process, and for several hours after treatment has ceased. In a real-world stimulation project using hydraulic fracturing,

3C seismograms 4000ms long sampled at 0.25ms from dozens of geophones may be recorded continuously for over 24 hours. Usually, there are no microseismic events of interest on the vast majority of the recordings.

When the microseismograms recorded by an array of 3C geophones have high signal-to-noise ratios (SNRs), hypocenter location using hodogram/back-azimuth analysis is straightforward and effective. However, in many cases involving well stimulation via hydraulic fracturing, the associated microseisms have very low magnitudes (about -2 to -3), and the consequent low SNRs severely limits the accuracy of the back-azimuth method. In this report, we present the results of various procedures developed to improve the accuracy of hypocenter location when the raw seismograms have low SNRs.

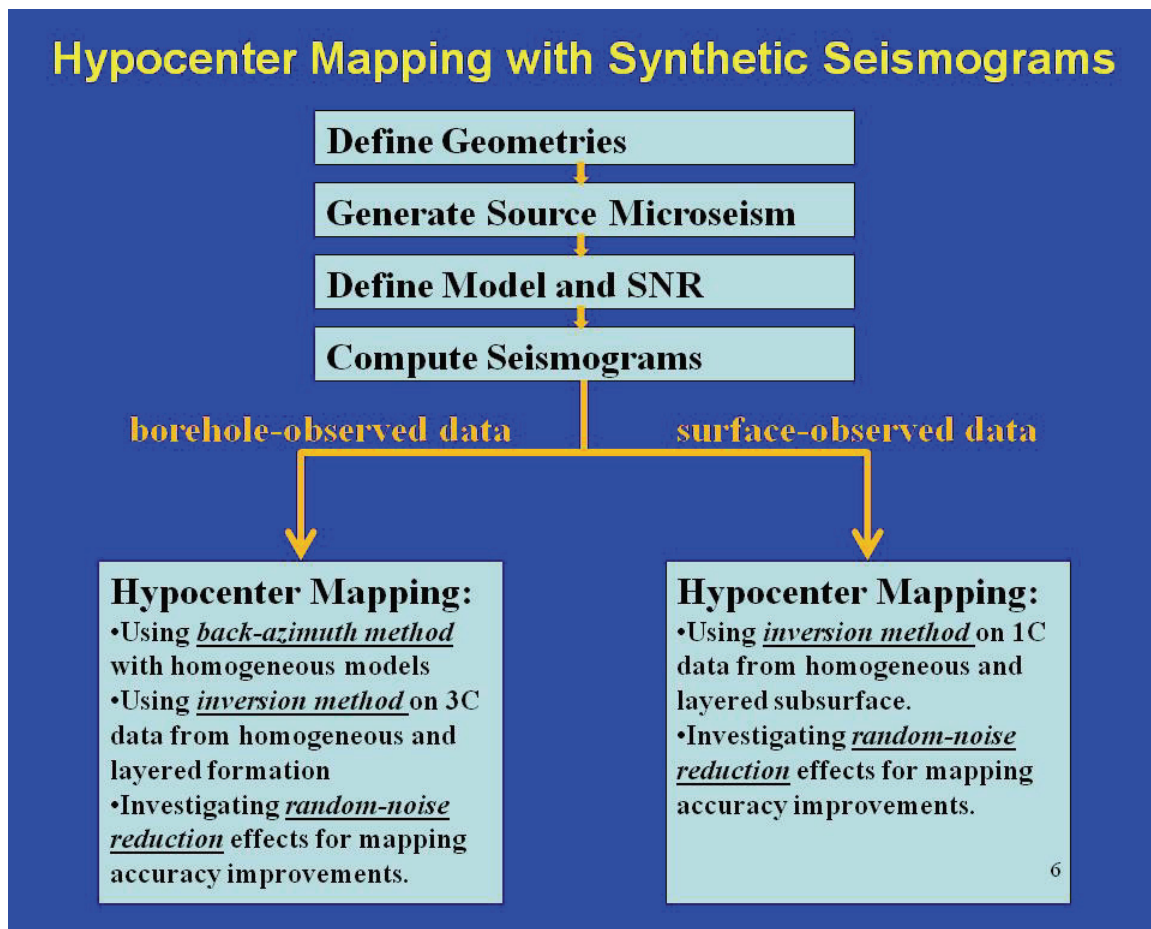


FIG.1: Outline of our research on microseismic monitoring and hypocenter mapping.

The outline of our research on microseismic analysis is shown on the Figure 1. We based our investigation on synthetic microseismograms for both well and surface 3C monitoring systems. In particular, we investigated how array geometry in vertical boreholes and SNR levels affect hypocenter location, and developed methods for mitigating the effects of noise and improving the mapping accuracy.

BACK-AZIMUTH METHOD WITH BOREHOLE-OBSERVED DATA

Figure 2 is a 3D representation of three monitoring wells surrounding a microseismic source. In general, the wells may be slanted with varying dips and azimuths. They may have horizontal sections. Figure 3 is a map view of the wells showing projections of the wells in the x-y plane.

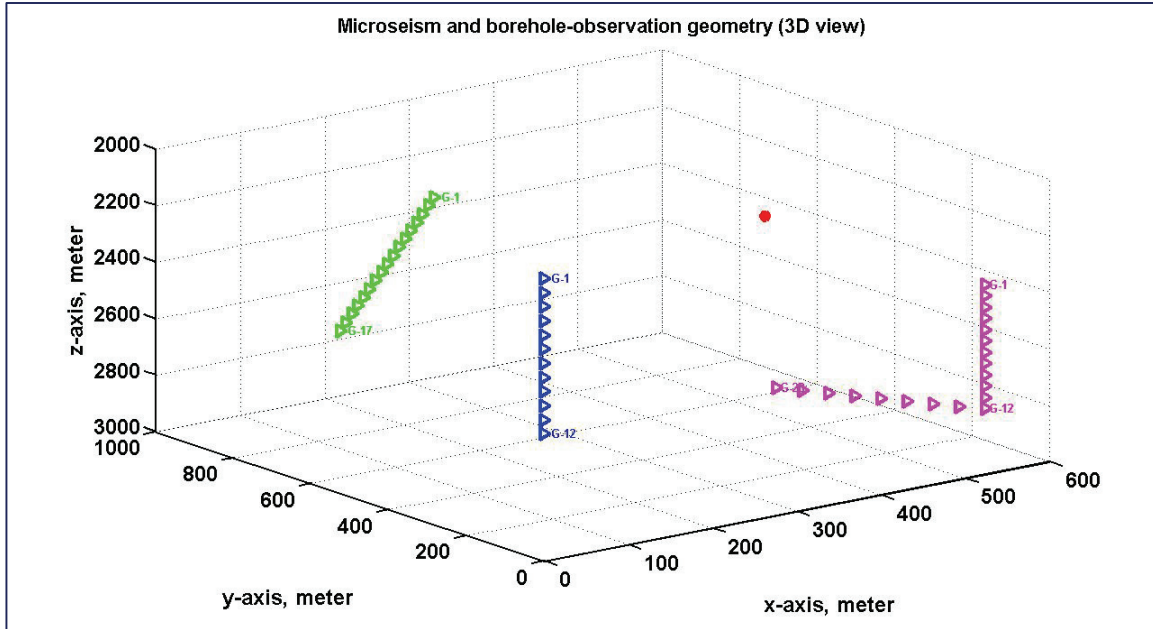


FIG. 2: Schematic 3D view of downhole triaxial geophones deployed in three observation wells surrounding a microseismic source (red dot).

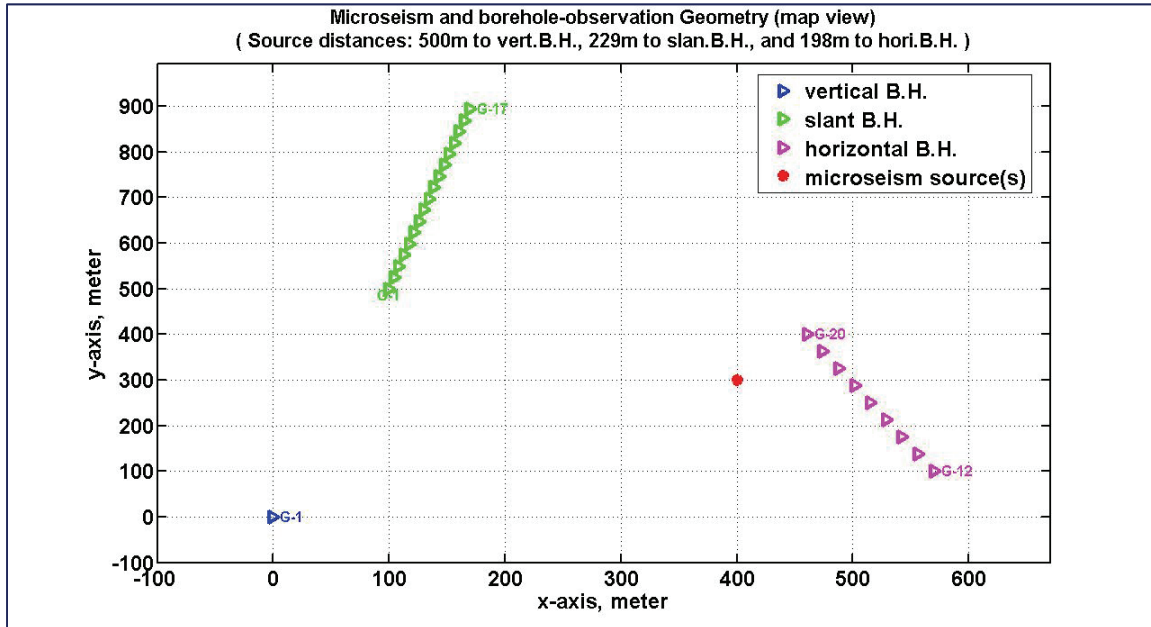


FIG. 3: Map view of the downhole triaxial geophones deployed in three observation wells.

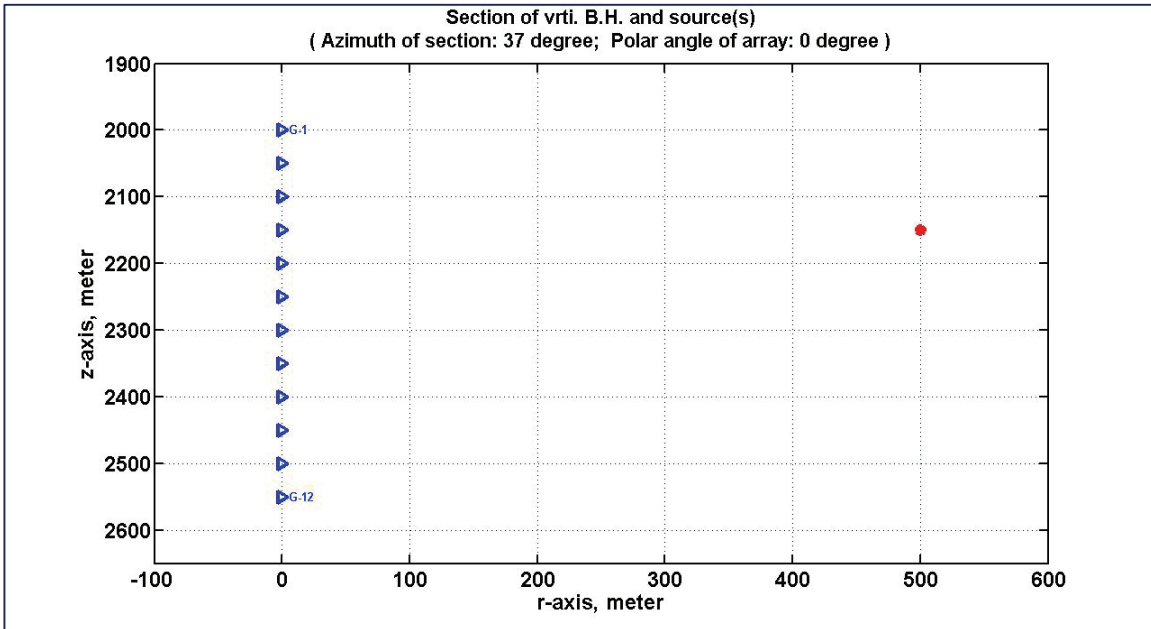


FIG. 4: Section view of an array of 12 3C geophones relative to a microseismic source (red dot). The spacing between geophones is 50 meters.

In this report, we have limited our investigations to a single vertical observation well. The vertical observation well with 12 downhole triaxial geophones and a microseismic source are shown schematically in section view on Figure 4.

GENERATION OF SYNTHETIC SEISMOGRAMS

For P and S arrivals, the absolute amplitudes of the x-y-z components at each geophone depend on the fracturing mechanisms and associated radiation pattern. The relative amplitudes of the x-y-z components at each geophone depend only on the propagation direction at the geophone. In this report, for simplicity, we will deal only with P-wave arrivals in a homogeneous and isotropic velocity field, so that the particle motion vector defined by the x-y-z components is parallel to the propagation direction or raypath, and points directly back to the microseismic source.

We generated synthetic seismograms with P-wave arrivals for the source-geophone geometry shown on Figure 4. Arrival times were calculated knowing the distance between the geophones and the microseismic source in the homogeneous 4000m/s velocity field. A minimum-phase source wavelet defined by

$$w(t) = \sin(2\pi f_0 t) \exp(-kt) ,$$

with $f_0 = 80\text{Hz}$ and $k = 50$, was sampled at 1ms. For a particular geophone, a base synthetic trace (1024ms long and sampled at 1ms) was produced by convolving the wavelet with a delta function located at the calculated arrival time. The amplitude of the base trace was scaled to account for spherical spreading. The x-y-z components were then derived from the scaled base trace by applying the direction cosines of the

propagation vector between the microseismic source and the geophone. Random Gaussian was then added to simulate different SNR levels. Figure 5 shows the resulting x-y-z traces with SNR=3 for the bottom geophone in the array of Figure 4, while Figure 6 displays the gather of 3C seismograms from all 12 geophones.

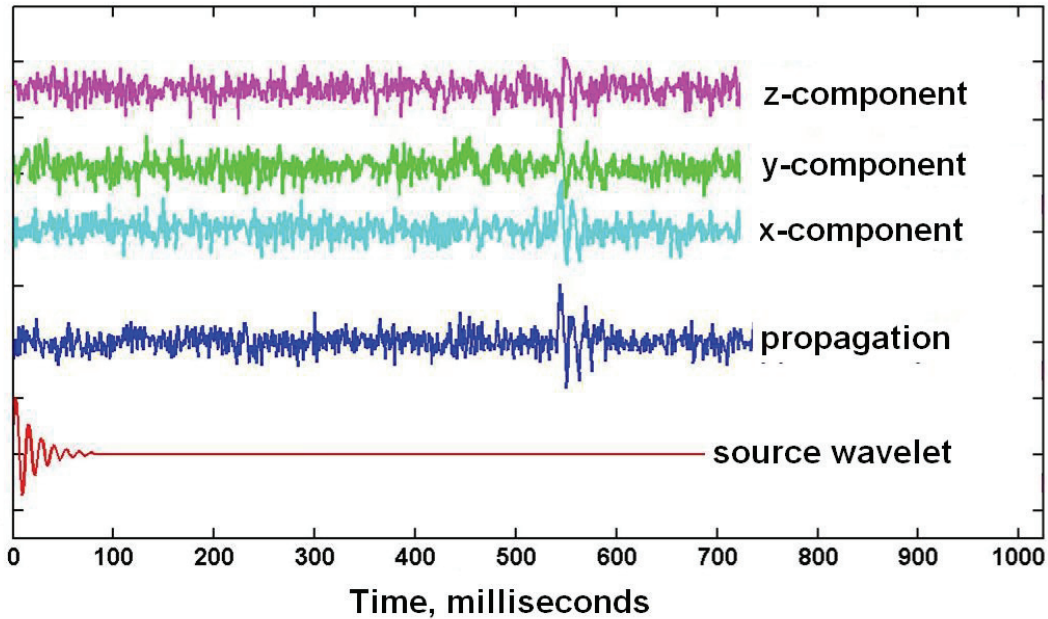


FIG. 5: Synthetic noisy 3C seismograms with SNR=3 for Geophone No. 12 on Figure 4. The dark blue trace shows the direct P arrival with particle motion along the propagation direction.

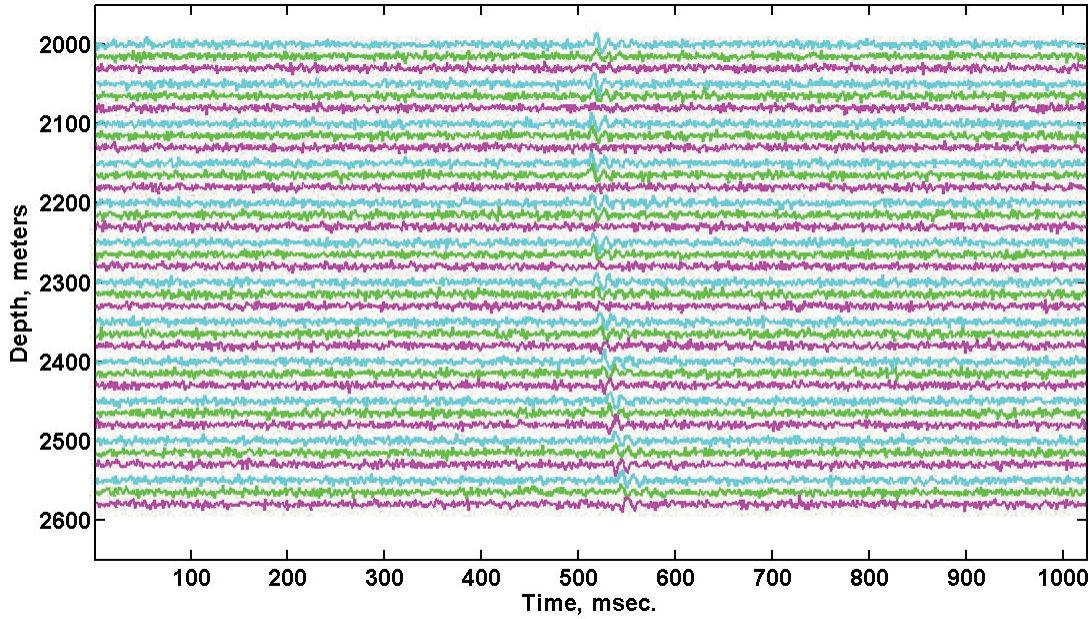


FIG. 6: Synthetic noisy 3C seismograms (SNR=3) for all 12 geophones in the array of Figure 4. Mauve trace is the z-component; green trace is the y-component, and cyan is the x-component.

HODOGRAM/BACK-AZIMUTH ANALYSIS FOR HYPOCENTER LOCATION

Now that we can generate 3C microseismograms knowing the source position, we address the reverse problem: how to locate the source knowing the 3C seismograms. In particular, we want to find the best estimate for the source coordinates when the seismograms are very noisy.

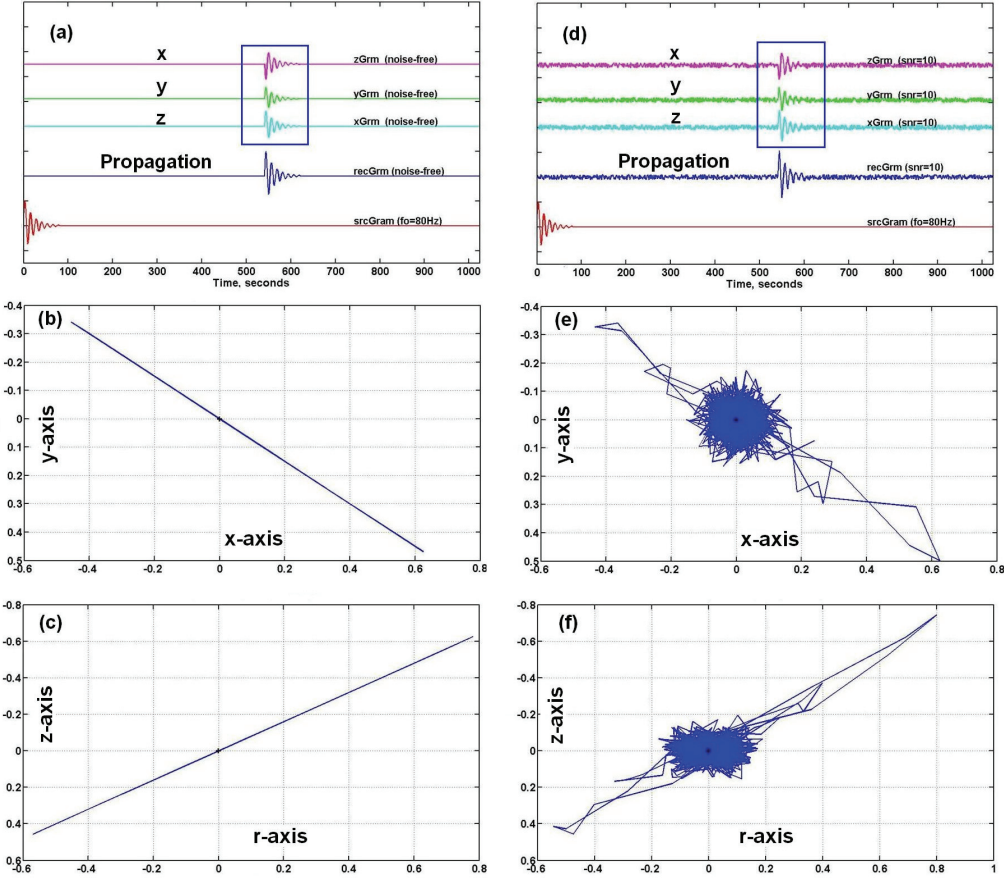


FIG. 7: (a) noise-free 3C seismograms; (b) map-view, and (c) section-view hodograms for SNR=0; (d) noisy 3C seismograms; (e): map-view, and (f) section-view hodograms for SNR =10.

To plot hodograms, we convert to cylindrical coordinates. If the x-y-z components of an arrival at geophone i are represented by $[g_x^i(t), g_y^i(t), g_z^i(t)]$, then the hodogram of the x-y components in the x-y plane (map view) is the parametric plot of $g_x^i(t)$ and $g_y^i(t)$ with time t as the parameter. Similarly, if we form a radial component

$$g_r^i(t) = [g_x^i(t)^2 + g_y^i(t)^2]^{1/2},$$

the hodogram in the z-r plane (section view) is the parametric plot of $g_r^i(t)$ and $g_z^i(t)$. Figure 7 shows the hodograms for clean and noisy 3C seismograms from the bottom geophone in the array. Only trace values within the small rectangles overlying the arrival are used to plot hodograms, meaning that time picking must be done before hodogram analysis. Time picking can be done using the modified energy ratio (MER) method of

Han et al. (2009). The front edge of the rectangles should be positioned close to the first break time of the arrival. The back edge should be two or three arrival cycles later.

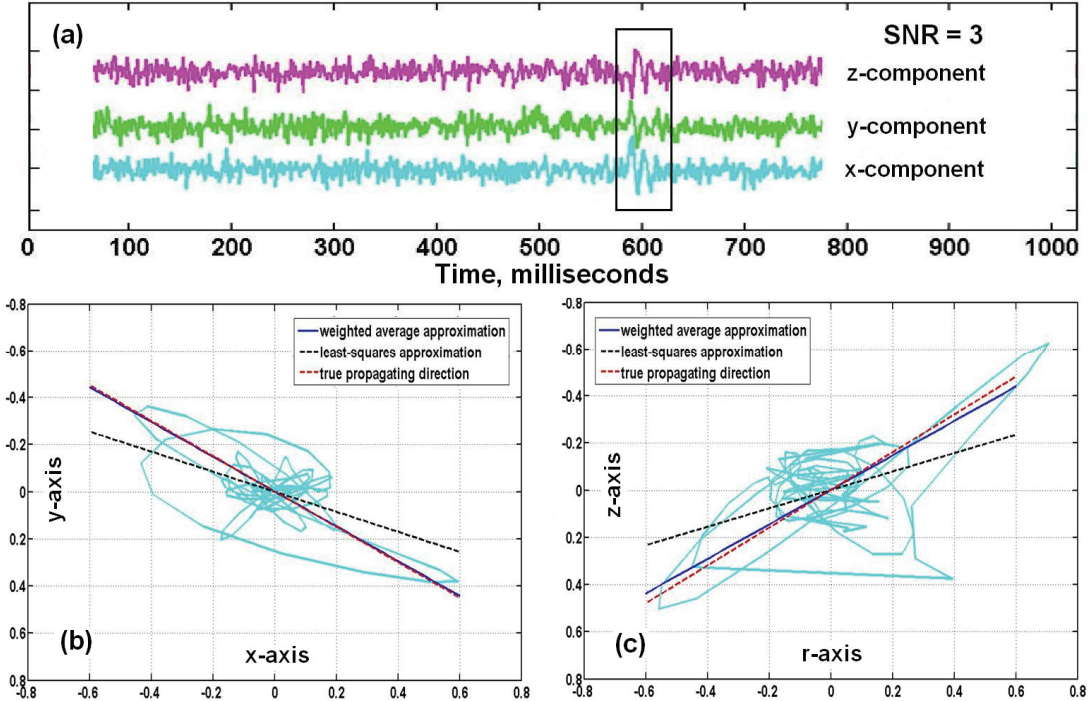


FIG. 8: (a) Synthetic noisy 3C seismograms for one geophone; (b) hodogram in map view; (c) hodogram in section view. Hodograms are time-parametric plots using seismogram points within the rectangle. Dotted red lines are along true propagation directions. Dotted black lines are along least-squares straight line fits of points on the hodograms. Solid black lines are along weighted averages of vectors defined by points on the hodograms.

For a homogeneous isotropic velocity field and P-wave arrivals, every pair of noise-free component values $[g_x^i(t), g_y^i(t)]$ at a given geophone defines a vector pointing directly at the source. If there is random noise, the vectors for all pairs also point toward the source but not exactly at it. However, an average of all vector directions counteracts the effects of the noise and is a reasonable estimate of the true slope.

The average slope can be calculated in two ways. We can find the least squares straight line fitting all the $[g_x^i(t), g_y^i(t)]$ pairs, and use the resulting slope as the average slope. We can also find the slopes of the individual $[g_x^i(t), g_y^i(t)]$ vectors and calculate a weighted average. The weighting is by the squared lengths of the individual vectors:

$$a_{xy}^i = \sum_{j=1}^m \{ (g_x^i(t)/g_y^i(t)) \cdot g_y^i(t)^2 \} / \{ \sum_{j=1}^m [g_y^i(t)]^2 \}. \quad (1)$$

A similar treatment of the component pairs $[g_r^i(t), g_z^i(t)]$ in the r-z plane gives the average slope a_{rz}^i for each geophone:

$$a_{rz}^i = \sum_{j=1}^m \{ (g_r^i(t) / g_z^i(t) \cdot g_R^i(t)^2) / \{\sum_{j=1}^m [g_R^i(t)]^2\} , \quad (2)$$

$$g_R^i(t) = [g_r^i(t)^2 + g_z^i(t)^2]^{1/2} .$$

Figure 8 shows examples of hodograms derived from noisy seismograms. These hodograms show significant deviation from linearity. The red dotted lines show the true propagation directions of the incoming wave. The black dotted lines have slopes from the least-squares straight-line fits to pairs of component values in the x-y and r-z planes. The solid blue lines have slopes estimated from the weighted averages of Equations 1 and 2. It is clear that the weighted average directions are closer to the true directions than the least-squares estimates.

HYPOCENTER MAPPING WITH BACK-AZIMUTH METHOD

The back-azimuth method locates hypocenters by back-projecting along incident raypaths whose directions are determined by hodogram analysis. In a homogeneous and isotropic velocity field, the back-projected raypaths in section view must all intersect at the source. The method finds the exact hypocenter coordinates (x_s, y_s, z_s) if no noise exists on the 3C seismograms recorded at the geophones (Figure 10).

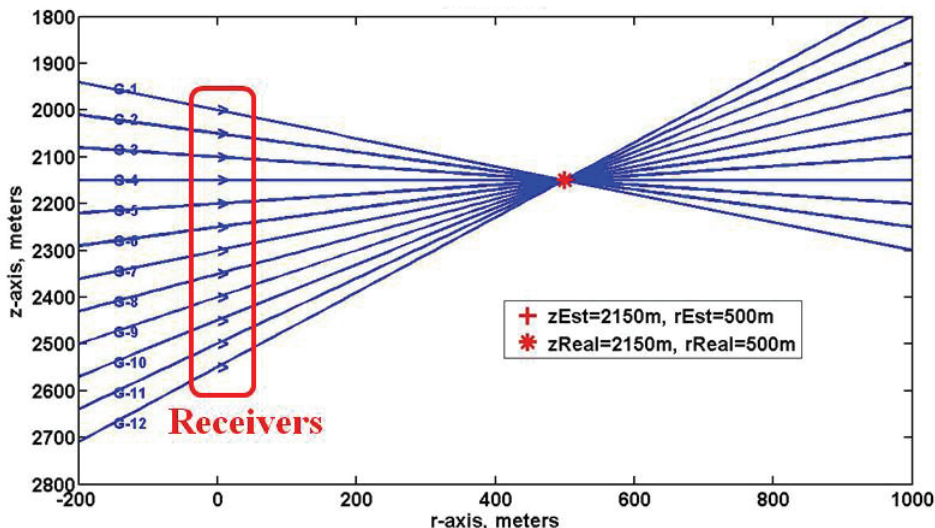


FIG. 9: Hypocenter mapping in section view for noise-free microseismograms. Blue lines are the raypaths determined from hodograms at each geophone. They intersect at one point that is exactly the hypocenter location.

For a homogeneous and isotropic velocity field, the propagation vectors determined at 12 geophones in a vertical array have identical azimuths in map view. In section view, the propagation vectors must all intersect at the same depth and radial distance. In particular, out of a set of 12 raypaths, combinations of pairs of raypaths must have identical intersection points. There are ${}_{12}C_2$ or 66 such combinations. For noisy data, the 66 intersections will be scattered randomly about the true intersection point. We can estimate the true intersection point by averaging the 66 pairs of (r_s, z_s) intersection coordinates. In map view, there will be 12 estimated azimuths, one for each of the geophones. A reasonable estimate for the true azimuth is the average. With an average radial distance r_s and an average azimuth, we can now estimate the (x_s, y_s) coordinates.

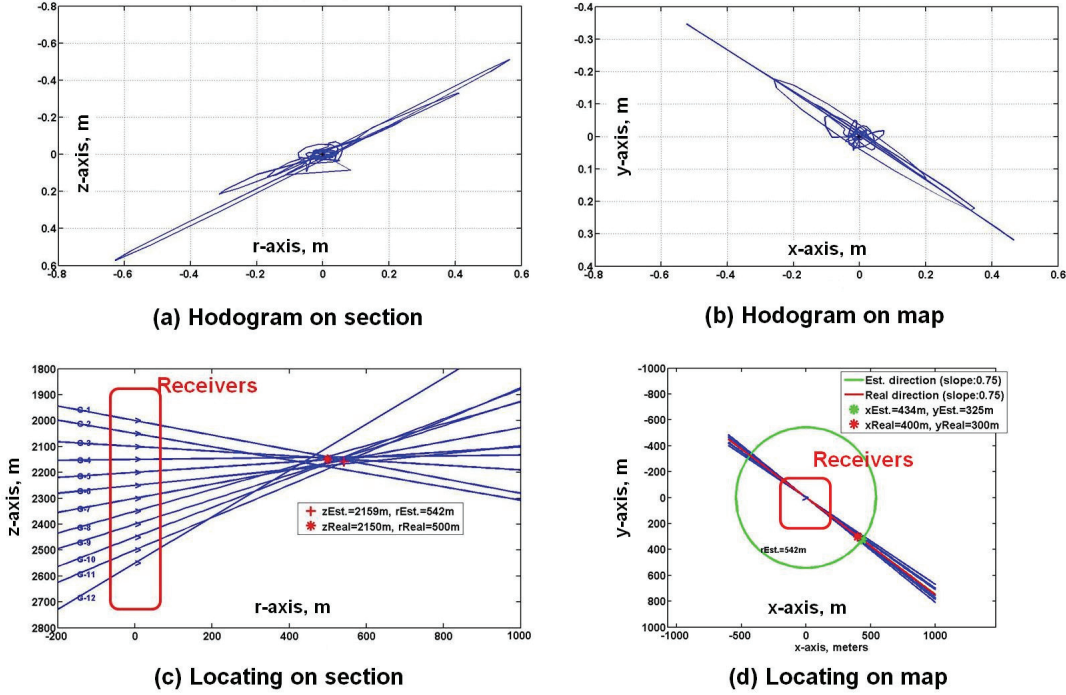


FIG. 10: Hypocenter location using back-azimuth method for 3C seismograms with SNR=10. The located (x_s, y_s, z_s) coordinates are (434m, 325m, 2159m). The true coordinates are (400m, 300m, 2150m).

Figure 9 summarizes the hodogram/back-azimuth method for locating a hypocenter using an example with noisy data (SNR=10) from 12 geophones. Figures 10(a) and (b) show hodograms at a single receiver, from which an average raypath direction can be derived. On the section view of Figure 10(c), the 12 raypaths with slopes estimated from Equation 2 do not intersect at a single point, nor do all the azimuths estimated from Equation 1 coincide on the map view of Figure 10(d). However, the average of 66 intersection coordinates on the section view gives $(r_s, z_s) = (542m, 2159m)$.

On the map view, the average of 12 x-y slopes is shown as the green line. When we draw a circle centered on the geophones with radius equal to the average r_s value (542m), its intersection with the line with the average slope gives (434m, 325m) as the estimated values for (x_s, y_s) . Thus, the hodogram/back-azimuth analysis, together with the various averaging procedures, has produced estimated source coordinates $(x_s, y_s, z_s) = (434m, 325m, 2159m)$. These are quite close to the true coordinates (400m, 300m, 2150m).

NOISE SUPPRESSION BEFORE HODOGRAM ANALYSIS

As we have seen on Figures 9 and 10, hodogram/back-azimuth analysis of low-noise P-wave arrivals is effective for hypocenter location. Hodograms are linear and align well with the propagation directions of the incident wave, leading to good estimates for the microseismic source coordinates. However, when raw seismograms have low SNR, we must suppress the noise before doing hodogram analysis.

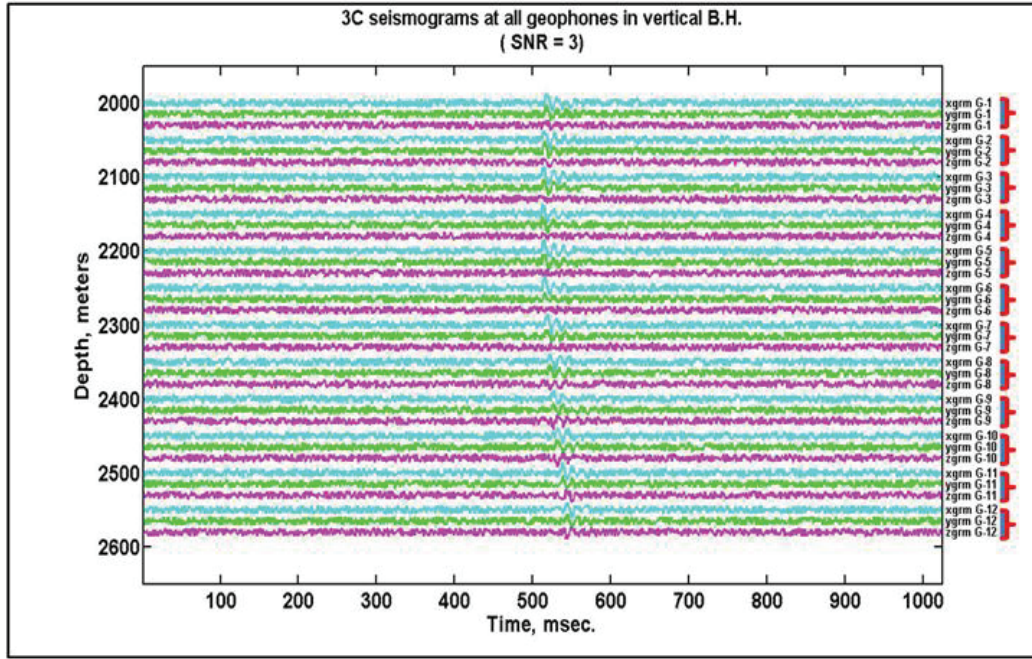


FIG. 11: Noisy 3C seismograms (SNR=3) from 12 geophones. Pre-processing must be done to attenuate the random noise on these traces prior to doing hodogram/back-azimuth analysis.

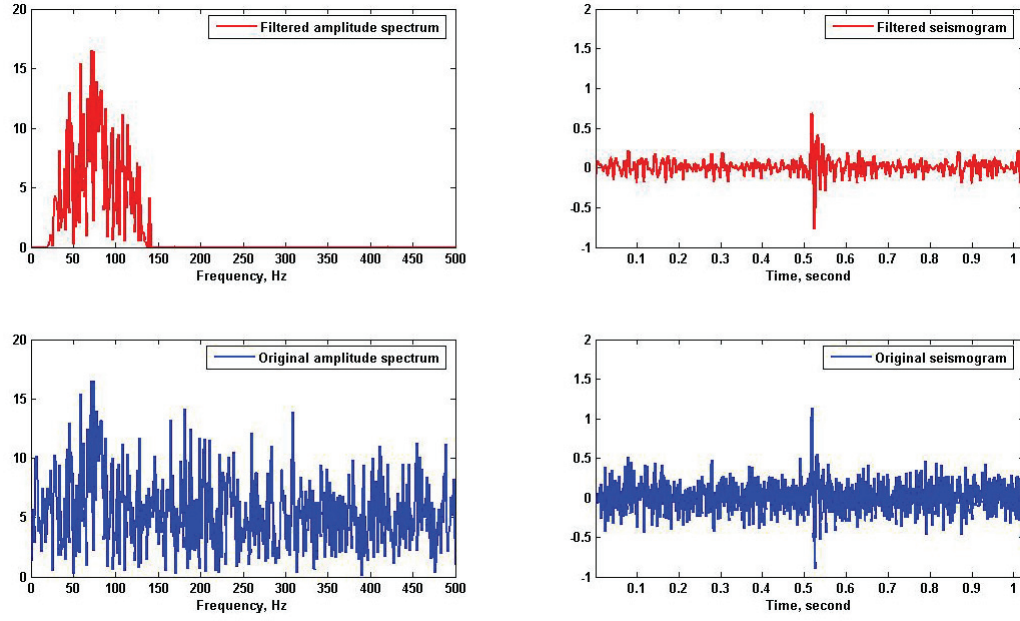


FIG. 12: Bandpass filtering to reduce random noise. The blue plots show the spectrum and trace for a raw seismogram with SNR of 3. The red plots are the results after applying a 20-40-120-140Hz Ormsby filter centered at the dominant signal frequency of 80Hz.

Figure 13 shows the trace and spectrum of a raw field seismogram with random noise before and after the application of an Ormsby filter centered on 80Hz, the dominant frequency of the arrival. We see that the level of random background noise has been

reduced by the filtering. The same filter was applied to all the seismograms on Figure 11. After frequency filtering, we applied time-domain windowing to isolate the arrivals.

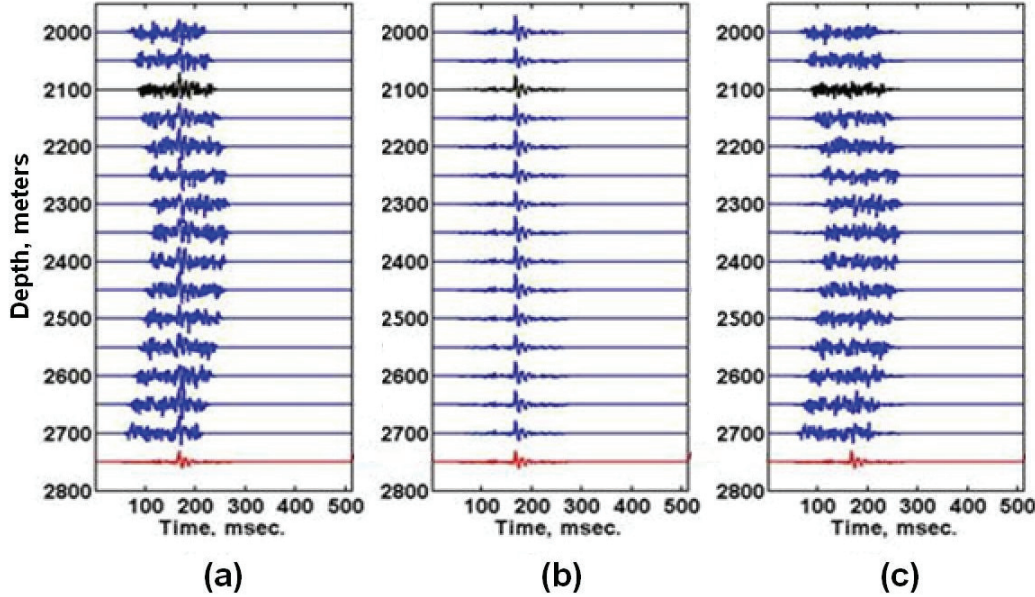


Fig.13: Noise-signal separation (NSS) for $\text{SNR} \approx 1.5$. (a) Original aligned seismograms; (b) noise-reduced separated signal components, and (c) separated Gaussian noise components. The red trace is the normalized average trace used as the reference for the separation process.

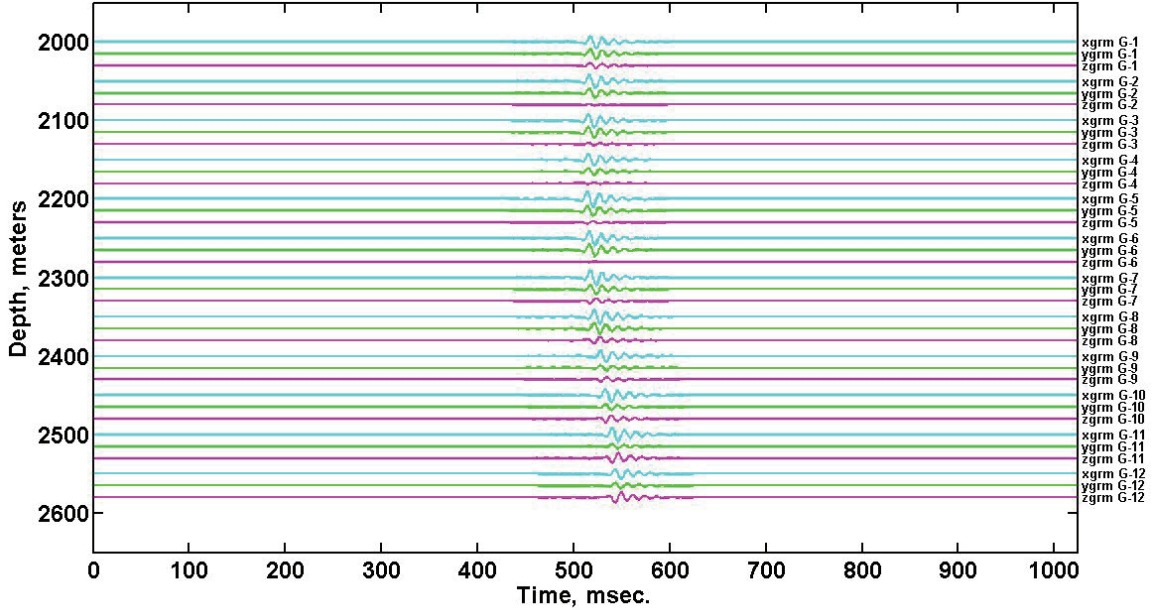


FIG. 14: The seismograms of Figure 12 after frequency filtering, windowing, and NSS. Compared to the raw unfiltered seismograms of Figure 12, the SNR is much improved.

We further reduced random noise using the noise-signal separation (NSS) method described by Han et al. (2009). NSS aligns the windowed component traces with the maximum amplitudes, and averages them to find a noise-reduced reference trace. The

dot product of the normalized reference trace with each of the 3C seismograms gives an amplitude coefficient. The coefficient is used as a scale factor with the reference trace to obtain a noise-reduced signal trace. By subtracting the noise-reduced signal trace from the original trace, we obtain a residual noise trace that shows little or no semblance to the reference trace. NSS reduces noises while preserving relative amplitudes of the analyzed traces (essential for the back-azimuth method to work). Figure 13 shows an example that summarizes the NSS procedure.

The seismograms from Figure 12, after frequency filtering, windowing, and NSS, are displayed on Figure 14. The random noise has been much reduced. The noise-reduced seismograms were then subjected to the hodogram/back-azimuth method for locating the microseismic hypocenter. The results are shown on Figures 15. The propagation directions on both section view and map view (i.e., dip angles and azimuths) of the derived raypaths are reasonably close to the true values.

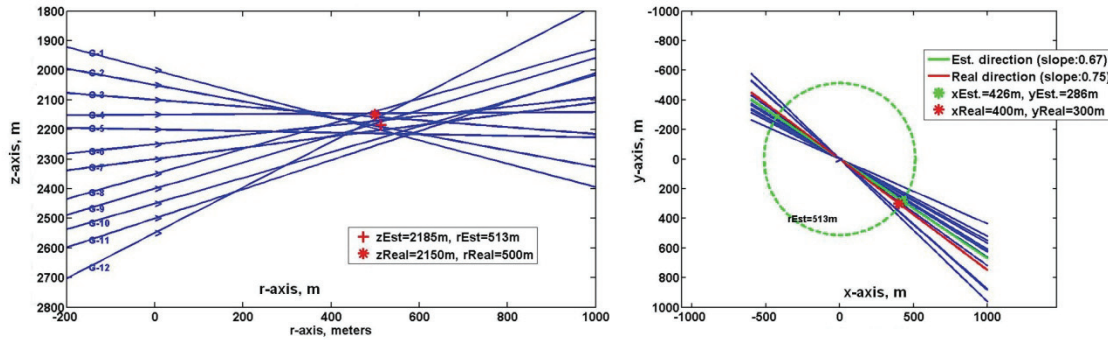


FIG. 15: Results of hodogram/back-azimuth analysis using the filtered, windowed, and noise-separated seismograms of Figure 14

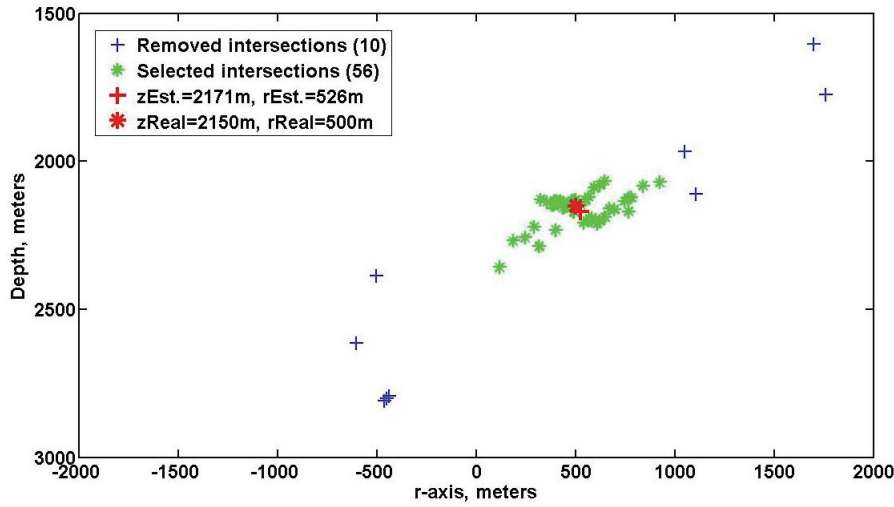


Fig. 16: Expanded scale section view of raypath intersection points for the data of Figure 14. The points, shown as blue crosses and green stars, are widely scattered. The blue crosses have been excluded when calculating the average intersection point (the red cross).

The expanded section view on Figure 16 shows that intersection points of the raypaths on section view are scattered, but they mostly fall between 0 and 1000m in the horizontal dimension. We used a simple clustering procedure to eliminate the obvious outliers. First we took an average of the (r_s, z_s) coordinates using all 66 intersections. We rejected those intersections lying beyond a certain number of standard deviations from the average, and recalculated a new average and standard deviation. This may be repeated, depending on how bad the original scatter is.

The final average was found using only the points denoted by green stars; the blue crosses have been excluded. Of the 66 intersections, 10 have been excluded. The average over the more tightly clustered subset of green intersection points gives a satisfactory final estimate of $(x_s, y_s, z_s) = (426\text{m}, 286\text{m}, 2171\text{m})$ for the hypocenter coordinates, close to true values of $(400\text{m}, 300\text{m}, 2150\text{m})$.

STATISTICAL ANALYSIS HYPOCENTER LOCATION ERRORS

We conducted a limited statistical investigation on how geophone spacings and noise levels affect the mapping accuracy of the back-azimuth method. Intuitively, we know that larger geophone spacings (resulting in larger recording apertures for the array) reduce location uncertainties. Also, we have observed that less noisy data produce more accurate estimates of hypocenter coordinates.

Table1: Average and standard deviation for hypocenter coordinates estimated using random-noise reduction and hodogram/back-azimuth analysis. R_{est} is the estimated radial distance.

Geophone Spacing	SNR=10				SNR=3				X _s =400m Y _s =300m Z _s =2150m R _s =500m
	X _{est}	Y _{est}	Z _{est}	R _{est}	X _{est}	Y _{est}	Z _{est}	R _{est}	
25m	381.3	295.4	2146.8	488.7	387.4	294.6	2146.5	473.1	Average (meters)
	28.06	11.37	3.74	17.38	51.68	54.17	14.15	62.37	Std. Dev. (meters)
50m	401.9	298.7	2148.9	501.4	414.2	310.3	2141.4	518.2	Average (meters)
	10.22	6.98	5.20	11.35	44.14	14.33	14.06	35.63	Std. Dev. (meters)

CONCLUSIONS

The back-azimuth method of locating microseismic hypocenters by back-projecting propagation vectors from 3C geophones works well in a homogeneous and isotropic velocity field if the 3C seismograms have high SNRs. The direction cosines of the propagation vector at a geophone are obtained by hodogram analysis of the 3C seismograms. When SNRs are low, good estimates for the hypocenter coordinates can still be found if we apply noise suppression techniques such as frequency filtering and noise-signal separation to the raw seismograms before performing hodogram analysis. We developed our version of the hodogram/back-azimuth method to include all these techniques. Extensive testing with synthetic data from a single vertical observation well indicated that the method is able to give reliable estimates of hypocenter coordinates using 3C microseismograms with SNRs as low as 3.5.

We performed a limited statistical study of how geophone spacing in a vertical and SNR levels affect the uncertainties in microseismic coordinates estimated from 3C seismograms using the hodogram/back-azimuth technique. The results of the study confirmed that uncertainties are decreased if recording angle apertures are large, and SNR levels are low. The findings support our research efforts into finding ways of suppressing noise in real microseismograms (Han et. al, 2009).

ACKNOWLEDGEMENTS

We express our gratitude to the industrial sponsors of CREWES and NSERC for supporting this research.

REFERENCES

- Block, L., Cheng, C.H., Fehler, M.C., and Phillips, S., 1994. Seismic imaging using microearthquakes induced by hydraulic fracturing: Geophysics, **59**, 102-112.
- Han, L., Wong, J. and Bancroft, J.C., 2009. Time picking and random noise reduction on microseismic data: CREWES Research Report, **21**, this volume.
- Maxwell, S. C. and Urbancic, T. I., 2001. The role of passive microseismic monitoring in the instrumented oil field: The Leading Edge, **20**, 636-639.
- Oye, V., and Roth, M., 2003. Automated seismic event location for hydrocarbon reservoirs: Computers and Geosciences, **29**, 851-863.